
Proceedings Paper:
Fan, Y. orcid.org/0000-0001-8038-7337, Zhang, L. orcid.org/0000-0002-4535-3200, Li, K. et al. (1 more author) (Accepted: 2024) Deep Learning-based EMI and IEMI Classification in 5G-R High-Speed Rail Wireless Communications. In: IEEE proceedings of The 2024 IEEE 99th Vehicular Technology Conference. IEEE VTC 2024, 24-27 Jun 2024, Singapore. IEEE . (In Press)

Deep Learning-based EMI and IEMI Classification in 5G-R High-Speed Rail Wireless Communications

Yejing Fan, Li Zhang, Kang Li, Minghan Bao
School of Electronic and Electrical Engineering
University of Leeds
Leeds, United Kingdom
Email: el17yf@leeds.ac.uk, L.X.Zhang@leeds.ac.uk, K.Li1@leeds.ac.uk, ml18m3b@leeds.ac.uk

Mowei Lu
Department of Engineering
University of Cambridge
Cambridge, United Kingdom
Email: ml2010@cam.ac.uk

***Abstract*—The proliferation of high-speed rail (HSR) networks and railway electrification has advanced the integration of the latest wireless communication networks with railway systems. Ensuring a reliable bidirectional communication link between moving trains and base stations is crucial to maintaining the safety of real-time rail operations. However, the growing complexity of railway systems and increased exposure to electromagnetic emissions present substantial challenges. In particular, railway wireless communication networks are vulnerable to various kinds of electromagnetic interference (EMI) and intentional EMI (IEMI), which could cause operational disruptions and safety hazards. This paper proposes a real-time classification method for EMI and IEMI, using deep learning-based bidirectional long-short-term memory (BiLSTM) networks. By employing multivariate time-series characteristics, the method can simultaneously learn both time and frequency information at a finer resolution, offering better performance than existing methods. The simulation results demonstrate a high accuracy of 93.4% and adaptability at different speeds and in various scenarios.**

***Index Terms*—Electromagnetic interference (EMI), Intentional EMI (IEMI), Deep Learning, Railway Wireless Communications**

I. Introduction

The expansion of High-Speed Rail (HSR) networks has significantly enhanced the mobility for passengers. Establishing a bidirectional connection between moving trains and base stations (BSs) is imperative to facilitate high uplink and downlink data rates while maintaining low latency during railway operations. The Future Railway Mobile Communication System (FRMCS), initiated by the International Union of Railways (UIC), signifies the transformation from the existing Global System for Mobile Communications-Railway (GSM-R) to the advanced 5G-Railway (5G-R). This evolution aims to provide automated and digitized services, aligning with stringent standards and specifications for reliability, availability, maintenance, and safety (RAMS) [1]. Although 5G standards have defined scenarios and use cases for Ultra-Reliable Low Latency Communication (URLLC), the propagation environment in HSR wireless transmission applications differs significantly from typical URLLC application scenarios [2]. Further, the complexity of the electrified railway system has reached unprecedented levels, raising concerns about its increased susceptibility of wireless transmissions to various electromagnetic interference (EMI) [3]. Given that the tolerance for EMI in HSR wireless communications is significantly lower than that in the public domain, it is vital to prioritize the research on EMI detection, ensuring operational safety for HSR networks.

EMI, unintentional or intentional, poses a critical challenge on HSR wireless communications relating to operating safety [4]. Electromagnetic signals, when superimposed on the communication signals at the receiver side, induce distortions that make the communication signals indecipherable. Such disturbances can lead to malfunctions of sensors and signaling systems, compromise the effectiveness of automatic train protection (ATP) systems, and cause errors within the radio module system, resulting in emergency braking events, congestion delays, and potential accidents. With the increasing accessibility of compact and discreet telecommunication devices in the public, it has become much easier for critical systems to be interrupted [3]. Notably, effective anti-jamming strategies for conventional wireless networks remain limited, let alone for HSR wireless communications. Additionally, specific railway environments, such as cuttings, viaducts, and tunnels, significantly affect the signal propagation characteristics. Consequently, it is imperative to devise a real-time EMI detection approach.

Current EMI detection methods, such as statistics-based detection and threshold-based approaches [5], face limitations when multiple indicators have to be assessed simultaneously. For the public cellular networks, several detection approaches are proposed, including binary and multiple classifications [6], [7]. The paper [8] uses the Bit Error Rate (BER) to demarcate the types of interference. However, the lack of evenly distributed data can lead to inaccurate threshold decisions. The latest jamming detection techniques have compared the performance among machine learning models, such as random forest (RF), aggregative hierarchical clustering (AHC), and support vector machine (SVM) [9]–[11]. Although these machine learning models demonstrate rapid data processing capabilities, they are restricted to analyzing the spectrum solely in the frequency domain. In addition, they do not address the challenges presented by dynamic HSR scenarios due to a lack of emphasis on time-series features. These models do not consider the time-frequency characteristics that are subject to variations in various dynamic HSR scenarios. This

limitation makes them less suitable for real-time detection.

To our knowledge, few studies have investigated EMI detection and classification for HSR wireless communications. Compared to the existing literature, this paper investigates multivariate time series features for classification and leverages the Long Short-Term Memory (LSTM) deep-learning method, which is useful for learning long-range dependencies. The system model is devised for the dynamic HSR scenario, where an on-board antenna captures downlink signals. The method demonstrates the effectiveness in detecting typical EMIs and IEMIs in real-time by learning temporal characteristics of signals from an extensive training dataset collected from diverse dynamic scenarios. Furthermore, the implementation of real-time EMI and IEMI classification will enhance the efficacy of mitigation strategies and signal resistance techniques. The main contributions of this paper are summarized below:

- A dynamic HSR scenario and three classes of potential wireless communication threats are constructed. Multivariate features are extracted and analyzed for both the time and frequency domains, with a finer resolution.
- The system, employing a BiLSTM deep learning algorithm designed for time-series characteristics, facilitates real-time EMI and IEMI detection and classification.
- The analysis framework can be scaled to a broad range of electrified transportation modes.

The rest of the paper is organized as follows. Section II gives an overview of the system model and the feature extraction. Section III introduces the LSTM and presents the BiLSTM-based classification algorithm. Simulation results are presented in Section IV, followed by the conclusion in Section V.

II. System Model

A. Overview of railway wireless communication networks

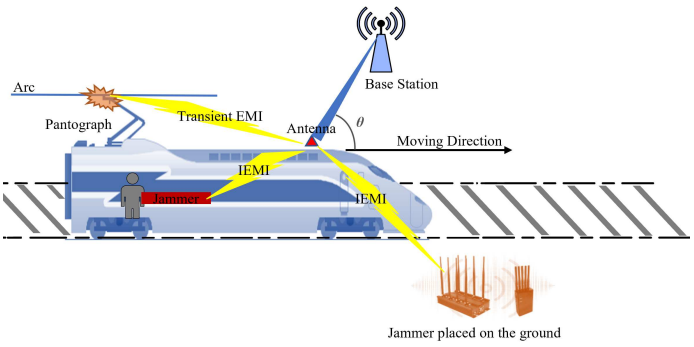

Fig. 1. The system model with three classes of EMI and IEMI in HSR wireless communications

The system model for HSR wireless communication, shown in Fig. 1, involves a macro BS operating at 1.9 GHz transmitting signals to a train antenna receiver fixed on the train roof. The chosen frequency band aligns with the 5G NR-based FRMCS requirements for latency and reliability [12]. In this paper, the total time is divided equally, and at the beginning of each time slot τ is for detection and classification. The distance between BS and the railway track is 100m. We assume that the high-speed train maintains constant speed as it approaches and moves away from the BS. The varying train-BS distances necessitate a dynamic and holistic system model formulation addressing rapid train movement and realistic signal propagation. This model includes:

- The Rician fading channel model is tailored for wireless environments featuring a dominant line-of-sight (LOS) component and multiple scattered paths, rendering it apt for dynamic scenarios like rural, viaducts, and tunnels.

$$P_r = A_1\sqrt{\frac{K}{K+1}}\cdot P_{t1}\cdot\left(\frac{\lambda}{4\pi d_1}\right)^2+\sum_{i=2}^{N} A_i\cdot P_{ti}\cdot\left(\frac{\lambda}{4\pi d_i}\right)^2 \tag{1}$$

  Here, P_r denotes the total received signal power, encompassing both LOS and Non-Line-of-Sight (NLOS) components. The constants A_1, K, P_{t1}, andd_1 are associated with antenna gains and system losses, Rician K factor, BS transmitted signal power, and distance for the first path, respectively. The summation term includes NLOS paths (2 to N), each characterized by parameters (A_i, P_{ti}, d_i), following a Rician distribution.
- The Doppler shift effect, arising from the train's movement relative to BS, causes a frequency shift in the received antenna signal, making it a crucial factor in HSR.

$$f_d = \frac{v\cdot f_c}{c} \tag{2}$$

  Here, f_d represents the Doppler shift, v is the velocity between the BS and the antenna, f_c is the carrier frequency of the transmitted signal from BS, and c is the speed of light. This equation describes the maximum shift when the relative direction of the train is parallel to the transmitted signal, i.e., when the angle θ is 0. This streamlines the system model without the need for detailed geometric information or angles.
- The Path loss model considers signal attenuation over large-scale distances in railway scenarios, employing the logarithmic distance model to capture changes in signal strength [13].

$$PL(d) = PL(d_0) + 10n\log_{10}\left(\frac{d}{d_0}\right) \tag{3}$$

  Here, $PL(d)$ is the path loss at distance d, $PL(d_0)$ is the path loss at the reference distance d_0, n is the path loss exponent, and d is the distance between the BS and the antenna.

B. Models of EMI and IEMI

a) Transient EMI: Transient EMI refers to short-duration EM disturbances in the radio frequency spectrum and can be caused by various sources during train operation, including pantograph-catenary arcing, electronic equipment on board, lightning strikes, power surges or other electromagnetic events. Transient EMI can be effectively modeled using damped sinusoidal signal characteristics.

$$V_{trans(t)} = A\left(e^{\frac{-t}{t_{rise}}} - e^{\frac{-t}{t_{hold}}}\right)\cdot sin(2\pi f_c t)\cdot\mu(t) \tag{4}$$

where A is amplitude, t_{rise} is rise time , t_{hold} is duration, and f_c is the center frequency of the superimposed useful signal. Fig. 2 shows the two consecutive transient interferences sharing similar characteristics but separated by variable time intervals. The time interval between two consecutive transient interferences, which refers to the repetition rate, may vary depending on operating conditions such as train speed, power supply line, and weather conditions. The unpredictable behavior of the repetition rate is similar to a random jammer device, alternating between active and idle states [9].

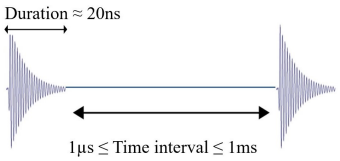

Fig. 2. Time representation of the transient EMI model

In the time domain, the signal exhibits a short-duration characteristic, while in the frequency domain , it possesses a broad spectrum overlapping the spectrum of the useful signal around 1.9 GHz frequencies. This makes some mitigation methods inapplicable, e.g., frequency-hop spread spectrum, diminishing the impact of specific frequency interference by sporadically hopping the data modulated carrier from one frequency to another.

b) In-train and On-ground Sweep IEMI: IEMI, also called jammers, can be defined as malicious wireless nodes placed by an adversary to cause intentional interference in wireless networks. Generally, there are multiple channels and frequency bands available for 5G railway high-speed wireless communications. As the low-cost jammer is constrained by its hardware circuit (e.g., very high ADC sampling rate and broadband power amplifier) to attack a large number of channels simultaneously, frequency sweep jamming attacks are used to circumvent this constraint [4]. This type of jammer launches an attack by transmitting a continuous high-power noise sweeping from one channel to another and repeating this process over time [14]. This type of jammer can be modeled as a cosine wave with random amplitude A that sweeps over a frequency band $[f1, f2]$ over a period of time T.

$$s(t) = Acos\left(2\pi\left(\frac{f_2 - f_1}{2T} \times t + f_1\right) \times t\right),\ 0 < t < T \tag{5}$$

In this model, the interference signal sweeps the frequencies around [1800,2000] MHz within a duration τ of 10 µs. This type of jamming signal is intentionally designed to disrupt the 1900 MHz frequency band of 5G-R.

Depending on the location of the IEMI, its impacts can vary. The system model considers two cases: IEMI originating from a portable device in a passenger's pocket inside the train or from a power source placed on the ground between the BSs [15]. In the first scenario, IEMI is generated inside the train, featuring consistent coupling conditions between the in-train jammer and the rooftop antenna. This coupling remains unaffected by train movement, passenger displacements, or local perturbations. Considering the shielding effectiveness of the train's structure in measurements (approximately 20 dB additional attenuation), the total estimated coupling loss combines the constant free-space loss and the shielding effectiveness attenuation. Fig. 3 depicts the time-frequency representation of the in-train sweep IEMI.

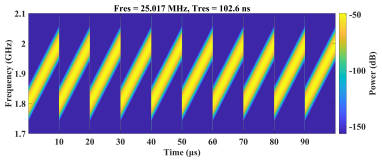

Fig. 3. Time-frequency representation of the in-train sweep IEMI

The second scenario involves placing the IEMI device on the ground. Given that the antenna is fixed on the roof of the train, the power received at the antenna is primarily affected by the movement of the train. To disrupt the useful signal, the jammer device is strategically placed to minimize obstacles in transmitting the jammer. This evaluation incorporates the two-ray LOS propagation model [16]:

$$P_r = P_t \frac{G_t G_r h_t^2 h_r^2}{d^4} \tag{6}$$

Here, P_r is the received power at the antenna, P_t is the transmitted power, G_t and G_r are the gains of the transmitting and receiving antenna, h_t and h_r are the heights of the transmitting and receiving antenna, and d is the distance between the jammer and the antenna. The power received by the antenna exhibits significant variation. As described in [15], one scenario involves a mere $10\ m$ distance from the jammer to the train antenna, especially if the device is placed close to the railway track or by a passenger waiting on a platform. This proximity results in a sufficiently large impact on the useful signal. The total estimated coupling loss considers both the Doppler shift and the two-ray LOS path loss. Fig. 4 depicts the time-frequency representation of on-ground sweep IEMI, capturing discernible power degradation that evolves over time as the train moves away from the jammer location.

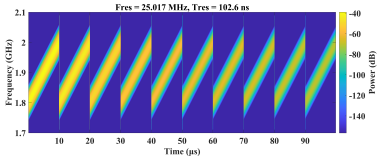

Fig. 4. Time-frequency representation of the on-ground sweep IEMI

III. Detection and Classification Algorithm

A. Long short-term memory (LSTM) basis

The LSTM network is an improved version of recurrent neural networks (RNNs) that addresses the vanishing and exploding gradients issues. It achieves this by introducing forgotten gates, input gates, and output gates, which enhance

the network's ability to selectively remember important information and forget irrelevant information. Detecting signals in 5G-R can be challenging, especially when the carrier frequency is 1.9 GHz. To satisfy the Nyquist theory, a practical sampling frequency of 5 GHz is employed. Consequently, within the signal detection window duration τ, the LSTM network is introduced into our algorithm to effectively capture features based on long time-series data.

B. Multivariate Time-Series Feature Extraction

When interference, characterized by a broad spectrum range with a short duration or a frequency sweep period, is introduced to the spectra, communication will be significantly impacted. It is possible to detect interference by monitoring changes in signal spectra received by the antenna.

The first group of time series features represents the frequency variations over time shown in Fig. 5. Generally in signal analysis, the shorter window with better time resolution can capture rapid changes for real-time detection, while the longer window with better frequency resolution can distinguish between different frequency components in the signal. In this paper, we divide the frequency band into smaller subbands and perform spectral analysis for each subband with a shorter window. This time-frequency decomposition approach allows the analysis of both the time and frequency information with finer resolution simultaneously. Specifically, the power level is computed based on 3D time-frequency spectrograms and the variance of power levels across 801 frequency points ranging from 1800 to 2000 MHz, with a frequency resolution of 250 KHz. By combining the results from all the subbands, a comprehensive time-frequency representation of the entire signal sequence is created to provide detailed insights into both frequency and time domain characteristics across a wide frequency range.

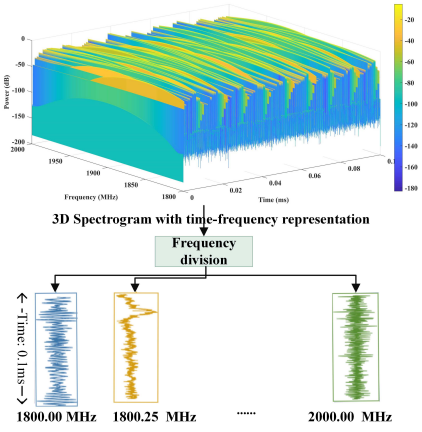

Fig. 5. Flowchart of the multivariate time-series feature extraction

The second group of time series features represents the amplitude variation of the signals received by the antenna. The third group of time series features is associated with spectral entropy, a concept derived from the Shannon information theory that measures the uncertainty and randomness of a signal power distributed across different frequencies. Overall, 803 distinct time series features are obtained and then into the deep learning algorithms. Consequently, the network learns these time series features simultaneously.

C. BiLSTM-based Multiclass Classification Algorithm

The BiLSTM-based multiclass classification algorithm, illustrated in Fig. 7, is trained using temporal features and corresponding labels. The BiLSTM layer plays a crucial role by incorporating both forward and backward information flow within the LSTM layers. The forward LSTM layers receive input at each specific time step, while the backward LSTM layers process the input in reverse order. Concatenating the outputs of these layers creates an encoded representation that combines both past and future information for each time step. This representation undergoes further processing in a fully connected layer for dimension reduction. The softmax activation function in the final layer transforms raw scores into a probability distribution across different classes, ensuring they sum up to 1. This probability distribution, denoted as Y_{ni}, is compared to the true label distribution T_{ni} using the cross-entropy loss formula [17] presented in Fig. 6. The formula measures the dissimilarity, specifically the negative log-likelihood, the negative log-likelihood between the predicted and true class distributions. Here, N is the total number of classes, and K is an index representing a specific class, ranging from 1 to N, corresponding to the different classes such as normal conditions, transient EMI, in-train sweep IEMI, and on-ground sweep IEMI. During training, the algorithm iteratively adjusts its parameters (weights and biases) to minimize the cross-entropy loss. This fine-tuning aims to enhance the model's ability to produce higher probabilities for the correct class and lower probabilities for other classes. During classification, the class with the highest probability in the output Y_{ni} is considered the predicted class. This decision is guided by the softmax function, which guarantees that the class with the highest raw score attains the highest probability.

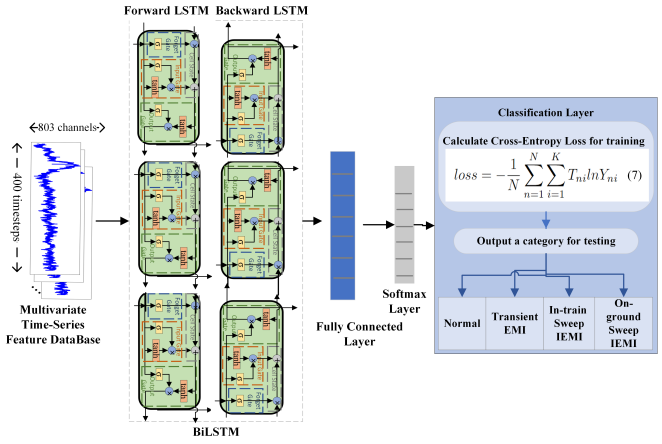

Fig. 6. Flowchart of the BiLSTM-based Classification Algorithm Structure

IV. Simulation Results and Analysis

The HSR wireless communication system model with Rician fading channel, Doppler shift, path loss, and ambient noise, provides a realistic platform for evaluating detection and classification systems under dynamic conditions. Data are collected as the train approaches and moves away from the BS with versatile speeds, within the coverage of one BS. The distance range from the train to the BS spans from 100 to a maximum of 2500 meters at a maximum speed of 450 km/h, with a maximum Doppler Shift of 792Hz.

Three types of interference are superimposed on the signals and collected within intervals containing multivariate time series features. These data fall into four classes: signals without interference, transient EMI, in-train sweep IEMI, and on-ground sweep IEMI. In the simulation, three different train speeds and three different scenarios (Rician Channel Fading K-factors and path loss exponents) are considered [18]–[21]. The simulations are conducted with a detection sampling interval of 100 μs every 1 second, covering a 20-second duration of train operation. A dataset comprises a total of 7,200 samples, and this dataset is divided into a training set of 70%, a validation set of 10%, and a test set of 20%. This allows the accuracy to be evaluated and facilitates the assessment of the adaptability of the performance in various scenarios and speeds. The parameters of the simulation and analysis are listed in the TABLE I.

TABLE I
Simulation Parameters

Parameter	Value
Carrier Frequency	1.9 GHz
Detection Bandwidth	1800 to 2000 MHz
Train Three Different Speed	250, 350, 450 km/h
Three Different Scenarios	Rural, Viaduct, and Tunnel
Rician K Factor	6, 3.66, 2.33
Path Loss Exponent	2.53, 3.5, 4
Ambient Noise Model	AWGN with SNR 20 dB
BS transmitted signal amplitude	1V
Output power jammer	1 W or +30 dBm
Deep learning optimizer	Adam
Initial learning Rate α	0.001
Mini-Batch Size	40

A. Performance Evaluation

a) Confusion Matrix: a table that summarizes the performance of a classification algorithm by comparing its predictions with the actual class labels in a data set. Based on the matrix shown in Fig. 7, the performance of our multi-classification model shows the test data set containing 1440 samples with a high accuracy over 93.4%. The errors primarily originate from undetected transient EMI. This implies that either no disturbance occurs within the 100 μs interval, or the pulse duration is too brief to be detected. Although the analysis process sets a high-resolution frequency up to GHz to capture the time characteristics for real-time detection, the minimal impact of transient EMI on the spectrogram remains a challenge to distinguish from normal conditions. Additionally, the in-train sweep IEMI can be erroneously identified as on-ground IEMI due to the similar sweep characteristics and variation in power level. Overall, the high accuracy across the four classes at different speeds and scenarios underscores the adaptability of our proposed algorithm,demonstrating robustness across varying HSR conditions.

Fig. 7. Confusion matrix of the multi-classification model on test set

b) Analysis and Comparison of Classification Accuracy: To further validate the effectiveness of the proposed method, we compared it with state-of-the-art methods, including RF, AHC, and SVM. Table II presents the performance comparison of all the methods in terms of classification accuracy. The observation reveals that deep learning-based models achieve superior performance compared to both traditional machine learning methods, such as RF (84.48%) and AHC (80.85%), and conventional data-driven models like SVM (84.4%). This underscores the significance of modeling the BiLSTM deep network structure to encode temporal information over sequences of data. Previous research based on SVM collected power level data from 801 frequency points within each spectrum [22]. However, it focused solely on the frequency domain, neglecting to consider frequency variance over time. Consequently, its performance may deteriorate with different train movement speeds and diverse scenarios, potentially posing safety concerns.

TABLE II
Classification Accuracy Achieved by the Compared Methods

Method	Normal	Transient EMI	In-train Sweep IEMI	On-ground Sweep IEMI	Average Accuracy
BiLSTM	100%	81.7%	100%	91.9%	93.4%
SVM	97.6%	80.94%	97.38%	86.67%	88.4%
RF	95.6%	74.25%	88.52%	79.56%	84.48%
AHC	91.24%	70.47%	86.06%	75.67%	80.85%

c) Receiver Operating Characteristic (ROC) Curve : ROC curve shows the true positive rate against the false positive rate at various classification thresholds, providing a visual representation of the trade-off between sensitivity and specificity of the model across different threshold values. A

higher ROC curve, closer to the top-left corner, with a larger area under the curve (AUC), indicates superior performance.

Since the ROC curve originates from binary classification, in this simulation, we employ the one-vs-all strategy. Each class is treated as the positive class, while the rest are treated as the negative class. This process is reiterated for each class, resulting in multiple ROC curves. The comparison with typical multi-classification methods, such as RF, AHC, and SVM, is illustrated in Fig. 8. As expected, the AUC value of the proposed BiLSTM-based algorithm is the highest at 0.9752 among the four algorithms, indicating superior capability in detection and classification. SVM acquires the second-highest AUC value, followed by RF and AHC. Overall, our proposed BiLSTM-based deep learning method addresses time-series data by analyzing both time and frequency characteristics simultaneously, achieving higher detection accuracy and adaptivity in varying attenuation scenarios, thereby proving more effective, especially when real-time detection and classification are crucial.

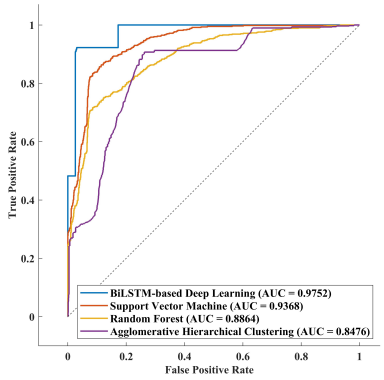

Fig. 8. ROC curves of multiclass-classification method comparison

V. Conclusion

In this paper, we develop a wireless communication model for a dynamic 5G-R HSR system. The model incorporates the dynamic channel propagation model, Doppler Shift, and large-scale path loss. Three classes of potential threats, namely transient EMI, in-train sweep IEMI, and on-ground sweep IEMI, are considered, and multivariate features are extracted for simultaneous analysis of both time and frequency domains. The BiLSTM-based deep learning algorithm effectively captures signals with time-series features, enabling real-time detection and classification. Simulations demonstrate that the model achieves a high detection accuracy of 93.4%, surpassing existing methods. Furthermore, the proposed method will facilitate the design of effective mitigation strategies and can be scaled to a broad range of electrified transportation modes.

References

[1] R. He, B. Ai, Z. Zhong, M. Yang, R. Chen, J. Ding, Z. Ma, G. Sun, and C. Liu, "5g for railways: Next generation railway dedicated communications," *IEEE Communications Magazine*, vol. 60, no. 12, pp. 130–136, 2022.

[2] L. Zhu, D. Yao, and H. Zhao, "Reliability analysis of next-generation cbtc data communication systems," *IEEE Transactions on Vehicular Technology*, vol. 68, pp. 2024–2034, 03 2019.

[3] S. Mili, V. Deniau, D. Sodoyer, M. Heddebaut, and S. Ambellouis, "Jamming detection methods to protect railway radio communication," *International Journal of Engineering and Innovative Technology - IJEIT*, vol. 4, no. 7, p. 7p, Jan. 2015.

[4] H. Pirayesh and H. Zeng, "Jamming attacks and anti-jamming strategies in wireless networks: A comprehensive survey," *IEEE Communications Surveys Tutorials*, vol. 24, no. 2, pp. 767–809, 2022.

[5] A. Marttinen, A. M. Wyglinski, and R. Jäntti, "Statistics-based jamming detection algorithm for jamming attacks against tactical manets," in *2014 IEEE Military Communications Conference*, 2014, pp. 501–506.

[6] Y. Arjoune and S. Faruque, "Smart jamming attacks in 5g new radio: A review," in *2020 10th Annual Computing and Communication Workshop and Conference (CCWC)*, 2020, pp. 1010–1015.

[7] K. Grover, A. Lim, and Q. Yang, "Jamming and anti–jamming techniques in wireless networks: a survey," *International Journal of Ad Hoc and Ubiquitous Computing*, vol. 17, no. 4, pp. 197–215, 2014.

[8] S. Dudoyer, V. Deniau, S. Ambellouis, M. Heddebaut, and A. Mariscotti, "Classification of transient em noises depending on their effect on the quality of gsm-r reception," *IEEE Transactions on Electromagnetic Compatibility*, vol. 55, no. 5, pp. 867–874, 2013.

[9] Y. Arjoune, F. Salahdine, M. S. Islam, E. Ghribi, and N. Kaabouch, "A novel jamming attacks detection approach based on machine learning for wireless communication," in *2020 International Conference on Information Networking (ICOIN)*, 2020, pp. 459–464.

[10] J. Villain, V. Deniau, A. Fleury, E. P. Simon, C. Gransart, and R. Kousri, "Em monitoring and classification of iemi and protocol-based attacks on ieee 802.11n communication networks," *IEEE Transactions on Electromagnetic Compatibility*, vol. 61, no. 6, pp. 1771–1781, 2019.

[11] J. Villain, V. Deniau, C. Gransart, A. Fleury, and E. P. Simon, "Characterization of ieee 802.11 communications and detection of low-power jamming attacks in noncontrolled environment based on a clustering study," *IEEE Systems Journal*, vol. 16, no. 1, pp. 683–692, 2022.

[12] Y. Fan, L. Zhang, and K. Li, "Emi and iemi impacts on the radio communication network of electrified railway systems: A critical review," *IEEE Transactions on Vehicular Technology*, vol. 72, no. 8, pp. 10 409–10 424, 2023.

[13] B. Ai, A. F. Molisch, M. Rupp, and Z.-D. Zhong, "5g key technologies for smart railways," *Proceedings of the IEEE*, vol. 108, no. 6, pp. 856–893, 2020.

[14] V. Deniau, C. Gransart, G. L. Romero, E. P. Simon, and J. Farah, "Ieee 802.11n communications in the presence of frequency-sweeping interference signals," *IEEE Transactions on Electromagnetic Compatibility*, vol. 59, no. 5, pp. 1625–1633, 2017.

[15] M. Heddebaut, V. Deniau, J. Rioult, and C. Gransart, "Mitigation techniques to reduce the vulnerability of railway signaling to radiated intentional emi emitted from a train," *IEEE Transactions on Electromagnetic Compatibility*, vol. 59, pp. 845–852, 06 2017.

[16] T. S. Rappaport, *Wireless communications: Principles and practice*. Prentice Hall, 1996.

[17] I. Goodfellow, Y. Bengio, and A. Courville, *Deep Learning*. MIT Press, 2016.

[18] M. Zhao, M. Wu, Y. Sun, D. Yu, S. Di, P. Zhou, X. Zeng, and S. Ge, "Analysis and modeling for train-ground wireless wideband channel of lte on high-speed railway," in *2013 IEEE 77th Vehicular Technology Conference (VTC Spring)*, 2013, pp. 1–5.

[19] Y. Liu, Y. Zhang, A. Ghazal, C.-X. Wang, and Y. Yang, "Statistical properties of high-speed train wireless channels in different scenarios," in *2016 IEEE 83rd Vehicular Technology Conference (VTC Spring)*, 2016, pp. 1–5.

[20] B. Ai, R. He, G. Li, K. Guan, D. He, G. Shi, and Z. Zhong, "Determination of cell coverage area and its applications in high-speed railway environments," *IEEE Transactions on Vehicular Technology*, vol. 66, no. 5, pp. 3515–3525, 2017.

[21] R. He, Z. Zhong, B. Ai, and J. Ding, "Distance-dependent model of ricean k-factors in high-speed rail viaduct channel," in *2012 IEEE Vehicular Technology Conference (VTC Fall)*, 2012, pp. 1–5.

[22] J. Villain, V. Deniau, E. P. Simon, C. Gransart, A. N. de São José, F. Valenti, and N. Becuwe, "Detection and classification of interference affecting lorawan communications in railway environment," in *2022 3rd URSI Atlantic and Asia Pacific Radio Science Meeting*, 2022, pp. 1–4.